Interferon-induced mechanosensing defects impede apoptotic cell clearance in lupus

Hao Li,[1] Yang-Xin Fu,[2] Qi Wu,[1] Yong Zhou,[3] David K. Crossman,[4,5] PingAr Yang,[1] Jun Li,[1] Bao Luo,[1] Laurence M. Morel,[6] Janusz H. Kabarowski,[7] Hideo Yagita,[8] Carl F. Ware,[9] Hui-Chen Hsu,[1] and John D. Mountz[1,7,10]

[1]Division of Clinical Immunology and Rheumatology, Department of Medicine, University of Alabama at Birmingham (UAB), Birmingham, Alabama, USA. [2]Department of Pathology, University of Chicago, Chicago, Illinois, USA. [3]Division of Pulmonary, Allergy and Critical Care Medicine, Department of Medicine, [4]Heflin Center for Genomic Sciences, and [5]Division of Genetics Research, Department of Genetics, UAB, Birmingham, Alabama, USA. [6]Department of Pathology, Immunology and Laboratory Medicine, University of Florida, College of Medicine, Gainesville, Florida, USA. [7]Department of Microbiology, UAB, Birmingham, Alabama, USA. [8]Department of Immunology, Juntendo University School of Medicine, Tokyo, Japan. [9]Infectious and Inflammatory Disease Center, Sanford-Burnham Medical Research Institute, La Jolla, California, USA. [10]Birmingham VA Medical Center, Birmingham, Alabama, USA.

Systemic lupus erythematosus (SLE) is a severe autoimmune disease that is associated with increased circulating apoptotic cell autoantigens (AC-Ags) as well as increased type I IFN signaling. Here, we describe a pathogenic mechanism in which follicular translocation of marginal zone (MZ) B cells in the spleens of BXD2 lupus mice disrupts marginal zone macrophages (MZMs), which normally clear AC debris and prevent follicular entry of AC-Ags. Phagocytosis of ACs by splenic MZMs required the megakaryoblastic leukemia 1 (MKL1) transcriptional coactivator–mediated mechanosensing pathway, which was maintained by MZ B cells through expression of membrane lymphotoxin-α1β2 (mLT). Specifically, type I IFN–induced follicular shuttling of mLT-expressing MZ B cells disengaged interactions between these MZ B cells and LTβ receptor–expressing MZMs, thereby downregulating MKL1 in MZMs. Loss of MKL1 expression in MZMs led to defective F-actin polymerization, inability to clear ACs, and, eventually, MZM dissipation. Aggregation of plasmacytoid DCs in the splenic perifollicular region, follicular translocation of MZ B cells, and loss of MKL1 and MZMs were also observed in an additional murine lupus model and in the spleens of patients with SLE. Collectively, the results suggest that lupus might be interrupted by strategies that maintain or enhance mechanosensing signaling in the MZM barrier to prevent follicular entry of AC-Ags.

Introduction

Systemic lupus erythematosus (SLE) and mouse models of lupus both exhibit a central feature of increased circulating apoptotic cell autoantigens (AC-Ags) and, in most cases, elevated type I IFN signaling produced by plasmacytoid DCs (pDCs) (1–3). The most accepted model is that the presence of uncleared ACs or AC-autoantibody immune complexes with DNA- or RNA-containing immune components can signal production of type I IFNs by pDCs. This in turn drives T cell activation and B cell maturation into autoantibody-producing B cells (4–8). Although it is well accepted that higher levels of circulating ACs can be due to decreased clearance of ACs in SLE and mouse models of lupus, the underlying mechanism for the clearance defect is not completely understood (2, 9–11). Marginal zone macrophages (MZMs) surrounding the splenic follicles have been reported to have the capability of both efficient clearance of ACs and induction of tolerance to AC-Ags (12–15). Because of the advantageous anatomic location of MZMs, they act as the final follicular AC-Ag exclusion barrier (2). We recently showed that in the BXD2 mouse model of autoimmunity, lupus is first associated with a spontaneous

decrease in the apoptotic debris clearance function and, later, with a loss in the number of MZMs surrounding the splenic follicles (2). Such a defect is associated with follicular translocation of AC-Ags bearing B cells to induce an AC-Ag–reactive T cell response (16–21). Interestingly, follicular translocation of marginal zone (MZ) B cells and marginal zone precursor (MZ-P) B cells can be promoted by type I IFN–induced upregulation of CD69, which prevents normal MZ localization of B cells by downregulating the chemotactic responses for sphingosine-1-phosphate (S1P) (20, 22).

Efficient and tolerogenic clearance of ACs by MZMs is a complex process requiring recognition of AC debris by scavenger receptors including macrophage receptor with collagenous structure (MARCO) and SIGN-R1, which send signals to the cytoskeletal apparatus of macrophages to promote proper engulfment and vesicular trafficking to phagolysosomes as well as induction of tolerogenic signals (23, 24). Defective serum-dependent, Rho-mediated mechanosensing cytoskeletal reorganization has been identified in macrophages obtained from 6 strains of lupus mice prior to disease onset (25). However, the molecular mechanism for the defects in mechanosensing signaling in lupus is not known.

Here, we describe how the maintenance of proper numbers and function of MZMs requires signaling through the lymphotoxin β receptor (LTβR) on MZMs by mLT-expressing MZ B cells. Importantly, type I IFNAR signaling on the MZ B cells results in mislocalization of MZ B cells into the follicle and disrupts crosstalk between MZMs and B cells. Signaling through LTβR on

MZMs is shown to regulate megakaryoblastic leukemia 1 (MKL1), a mechanosensing transcriptional coactivator maintaining MZM homeostasis in the MZ as well as AC phagocytosis and clearance by these MZMs (23, 24, 26–31). Dissociation between MZMs and mLT+ B cells was shown in 2 strains of lupus-prone mice, BXD2 (17, 32–37) and B6.Sle1.Sle2.Sle3 (B6.TC) (38). Diminished expression of MKL1 as well as loss of MARCO+ cells associated with follicular translocation of CD1c+ MZ B cells were similarly identified in the spleens of SLE patients. The results reported herein may therefore be more generally applicable, as they identify an important defect associated with lupus.

Results

Decreased MARCO+ macrophages and increased pDCs are common features of lupus in both humans and mice. A common feature of SLE in both human and mouse models of SLE is decreased clearance of ACs and increased production of type I IFNs by pDCs (1–3, 6, 9–11, 13, 14, 39). We and others have previously shown that physical deletion or spontaneous loss of MARCO+ MZMs resulted in defective AC clearance (2, 12–15, 40, 41) and that such a defect is associated with the development of lupus in susceptible mouse models (2, 42). We analyzed the distribution of MARCO+ cells in the spleens of non-SLE controls (*n* = 6) and in the spleens pf patients with SLE (*n* = 5) and found a dense layer of MARCO+ cells in the perifollicular regions in all non-lupus control spleens; however, this layer of MARCO+ cells was significantly reduced in all SLE spleens (Figure 1A). In contrast, we observed a dense layer of PDCA1+ pDCs in the splenic perifollicular region in SLE patients, and this dense pDC layer was significantly diminished in the same region in control spleens (Figure 1B).

A similar reciprocal distribution of low numbers of MARCO+ MZMs (Figure 1C) and dense aggregation of PDCA1+ pDCs (Figure 1D) were identified in the splenic MZ in 2 different strains of lupus-prone mice, BXD2 and B6.TC. Production of type I IFNs by pDCs could be stimulated by mammalian nucleic acids derived from apoptotic debris as a result of AC clearance defects (43). pDCs accumulated in the splenic MZ in 3-month-old BXD2 and B6.TC mice, but MZM loss became prominent in 11-month-old mice (Figure 1, C and D), suggesting that type I IFNs may play an important role in orchestrating the loss of MZMs. Indeed, a deficiency of IFNAR in BXD2 (BXD2-*Ifnar*−/−) mice rescued the age-related loss of MZMs (Figure 1C), prevented the aggregation of pDCs in the splenic MZ (Figure 1D), and also diminished spontaneous germinal centers (GCs) in the spleen and autoantibody sera titers of BXD2 mice (Supplemental Figure 1, A and B; supplemental material available online with this article; doi:10.1172/JCI81059DS1). Together, these findings suggest that loss of MZMs and accumulation of pDCs exhibit a reciprocal association in both human and mouse spleens and that enhanced IFNAR signaling may dissipate critical AC phagocytic MZMs in the splenic MZ to promote lupus in BXD2 mice.

Type I IFN induces loss of MZMs via follicular translocation of mLT+ B cells from the MZ. To determine whether increased IFNs acted directly on MZMs to result in their reduction, BXD2-*Rag1*−/− mice were reconstituted with BM from either GFP+ BXD2-*Ifnar*+/+ or GFP− BXD2-*Ifnar*−/− mice. The number of pDCs and expression levels of type I *Ifn* genes in BXD2-*Rag1*−/− mice and WT BXD2 mice were comparable (Supplemental Figure 2), making it possible to assess the effects of pDCs and type I IFNs in these recipients. MZMs were quantitated by F4/80−CD11b^int^SIGN-R1^hi^ and I-A^b−^ macrophages. Four months after the transfer, there was no difference in the percentage of MZMs, whether they were derived from IFNAR+ or IFNAR^null^ donors (Figure 2A). However, confocal image analysis revealed that IgM^hi^ B cells derived from IFNAR+ mice had predominately translocated into the follicle, whereas IgM^hi^ B cells from IFNAR^null^ mice were predominantly localized in the MZ (Figure 2, B and C), suggesting that defective retention of MZ B cells in the MZ can be an important factor leading to the loss of MZMs in IFNAR-intact BXD2 mice.

The importance of MZ B cells in maintaining MZMs was verified using an antibody directed against the NOTCH2 ligand delta-like 1 (anti-DLL1) to block NOTCH2-DLL1 interaction (44), a signal needed for MZ B cell development. We showed that normal MZM numbers (Supplemental Figure 3, A and B) in both B6 and BXD2 mice were significantly reduced by specifically depleting CD1d+CD23− and CD21+CD23− MZ B cells (Supplemental Figure 3, C and D) in anti-DLL1–treated mice (44). As NOTCH2 is mainly expressed by MZ B cells, but not MZMs (Supplemental Figure 3, E and F), these results suggest that, as in B6 mice, maintenance of MZMs in the splenic MZ of BXD2 mice requires MZ B cells.

The expression of mLT by B cells has been implicated in the maintenance of MZMs (45–51). As type I IFNs exhibit an important property for the promotion of follicular translocation of MZ B cells (Figure 2, B and C, and refs. 20, 21, 42), we analyzed whether there was mislocation of mLT+ B cells in the spleens of BXD2 mice. FACS analysis confirmed that in B6, WT BXD2, and BXD2-*Ifnar*−/− mice, mLT was highly expressed on MZ and MZ-P B cells (Figure 2D). Confocal image analysis showed that in B6 and BXD2-*Ifnar*−/− mice, the majority of the mLT+CD1d+ B cells were located in the MZ (Figure 2, E and F). However, in the spleens of WT BXD2 mice, the majority of mLT+CD1d+ B cells were located in the follicle (Figure 2, E and F). The essential role of mLT+ B cells in the maintenance of MZMs was verified by analysis of MARCO+ MZMs in in *Ltb*^fl/fl^ *Cd19-Cre* B6 mice, which lack mLT specifically on the surface of B cells (51). *Ltb*^fl/fl^ *Cd19-Cre* B6 mice exhibited a significant decrease in MARCO+ MZMs (Figure 2G), which was further confirmed using FACS analysis by gating on the F4/80−CD11b^lo^I-A^b−^SIGN-R1+ subpopulation (Figure 2H). These results suggest that lack of mLT+ B cells or lack of mLT+ B cell retention in the MZ as a result of IFNAR-dependent follicular translocation leads to loss of MZMs.

Loss of LTβR leads to loss of MZMs and enables development of GCs. LTβR signaling in endothelial cells (ECs) has been suggested to play an important role in high endothelial venule formation (50), which may then affect MZ organization. Further, signaling provided by mLT+ B cells has been shown to play an important role in the formation of a GC response through interactions between B cells and follicular DCs (FDCs) (48). Our results thus far, however, suggest a concept in which mLT+ B cells support both the MZ and GC structures, depending on their anatomic location. We generated *Ltbr*^fl/fl^ *Lys-Cre* B6 mice to determine whether loss of LTβR signaling on macrophages, but not ECs or FDCs, perturbs MZMs without affecting GC formation. We found that splenic MZMs in 1-month-old *Ltbr*^fl/fl^ *Lys-Cre* B6 mice were fully developed (Figure
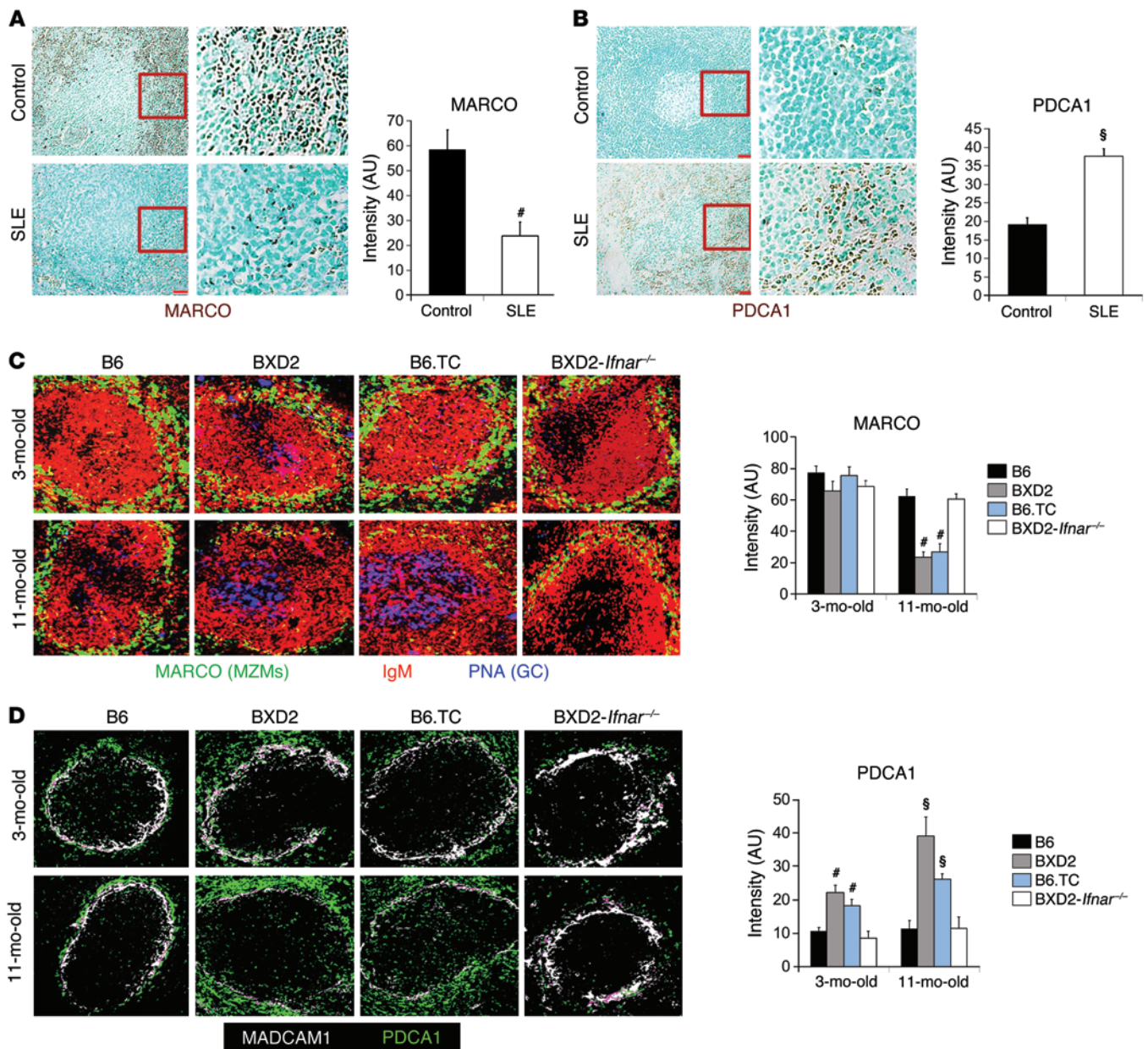
Figure 1. Decreased spleen MZMs and increases pDCs as a common feature of lupus. (**A** and **B**) IHC staining and intensity quantitation of MARCO⁺ cells (**A**) or PDCA1⁺ pDCs (**B**) in the spleens of normal ($n = 6$) versus SLE ($n = 5$) individuals. Representative images of spleen follicles. Original magnification, ×20. Boxed areas in the left panels were digitally magnified and are shown in the right 2 panels. Bar graphs show ImageJ intensity quantitation of 10 randomly selected splenic perifollicular regions per section. (**C** and **D**) Spleens obtained from B6, BXD2, B6.TC, and BXD2-*Ifnar⁻/⁻* mice at 3 and 11 months of age were analyzed. Representative confocal microscopic images of (**C**) PNA (blue), IgM (red), and MARCO (green), and (**D**) MADCAM1 (white) and PDCA1 (green) for representative splenic follicles. Original magnification, ×20. Bar graphs show ImageJ intensity quantitation of 10 randomly selected spleen MZ regions per section. Data represent the mean ± SEM. All images are representative splenic regions or splenic follicles (#$P < 0.01$, §$P < 0.005$ vs. control or B6, Student's *t* test; $n = 2$–3 mice per group for 2 independent experiments).

3A). However, the percentage of MZMs was reduced in 4-month-old *Ltbr^fl/fl^ Lys-Cre* B6 mice compared with the percentage detected in B6-*Ltbr^fl/fl^* mice (Figure 3, A and B). The essential role of LTβR⁺ expression on MZMs in preventing autoimmunity was confirmed by the observation that *Ltbr^fl/fl^ Lys-Cre* B6 mice gradually developed features of autoimmunity, including the accumulation of uncleared TUNEL⁺ ACs in the MZ (Figure 3C), elevated levels of serum malondialdehyde (MDA), a lipid antigen derived from ACs (ref. 1 and Figure 3D), spontaneous formation of GCs (Figure 3, A,

C, and E), and a relatively small, yet statistically significant, elevation of IgG autoantibody serum titers (Figure 3F).

LTβR signaling maintains MKL1 expression in MZMs. The above results suggest that elevated IFNAR signaling and the lack of LTβR signaling in the splenic MZ exhibited a similar deleterious effect on MZMs. To determine the molecular mechanism by which LTβR signaling maintains MZMs, BXD2 mice were treated with either control PBS or LTβR-Fc to block LTβR signaling. GeneChip analysis of MZMs indicated that a predominant signaling modification
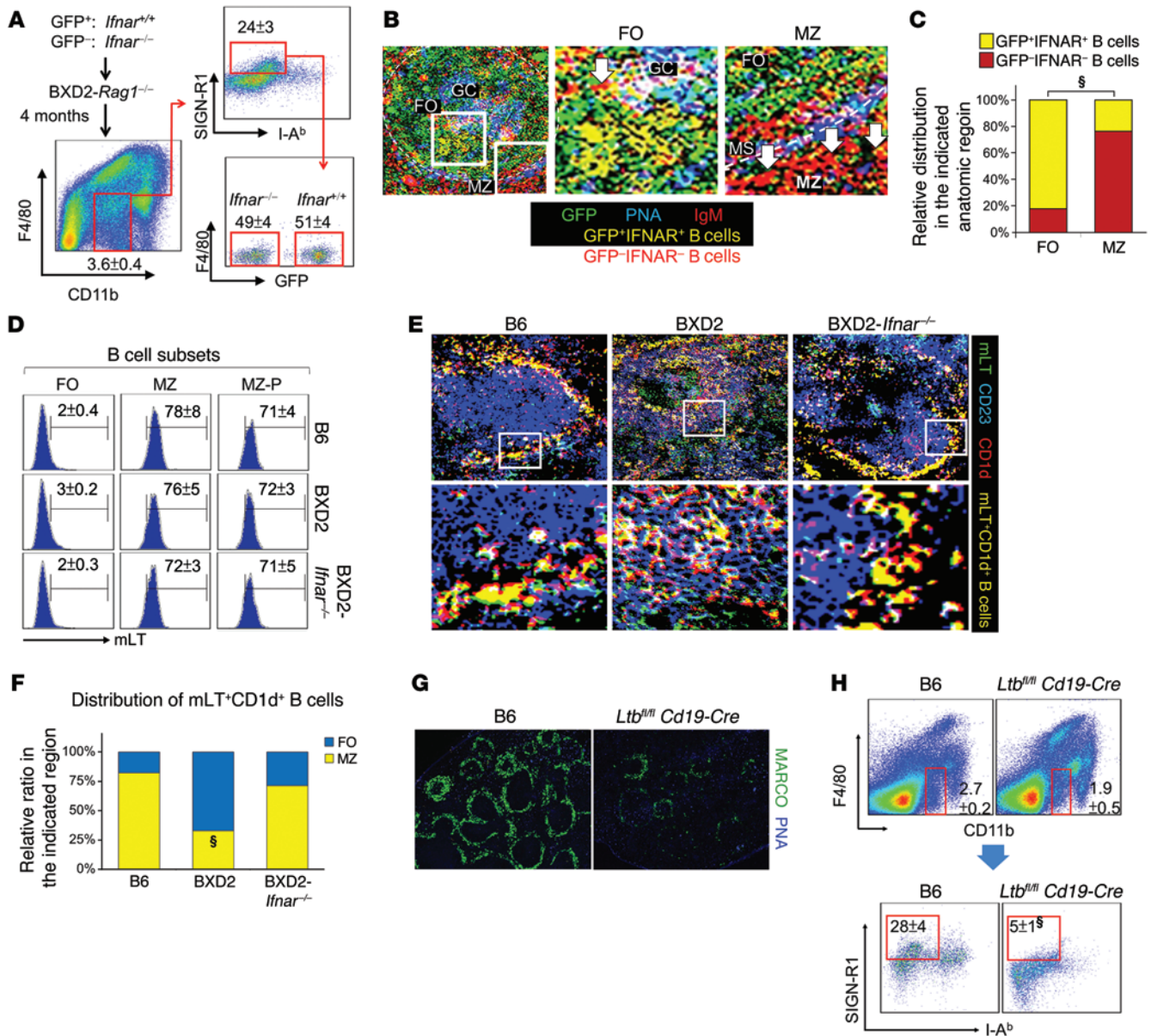
Figure 2. Type I IFN indirectly promotes dissipation of spleen MZMs via follicular translocation of mLT⁺ B cells. (A–C) Mixed BM chimeric mice were generated by reconstitution with 1:1 GFP⁺ *Ifnar⁺/⁺* plus GFP⁻ *Ifnar⁻/⁻* BM cells into BXD2-*Rag1⁻/⁻* mice (5-month-old) and analyzed 4 months later. **(A)** FACS analysis of the percentage of MZMs (F4/80^{neg}CD11b^{lo}SIGN-R1⁺I-A^{b-}) derived from GFP⁺ *Ifnar⁺/⁺* and GFP⁻ *Ifnar⁻/⁻* donors. **(B)** Confocal microscopic images show the distribution of transferred donor cells. Original magnification, ×20; boxed areas in the left panel were digitally magnified and are shown in the right 2 panels (white arrows point to GFP⁻IgM⁺IFNAR⁻ red B cells). MS, marginal sinus. **(C)** Quantitation of the distribution of GFP⁺ and GFP⁻ donor cells in either follicles or the MZ of the recipient spleens (χ^2 test). Five randomly chosen areas were counted for each follicle. **(D)** FACS analysis of mLT expression on follicles (IgM^{lo}CD21^{lo}CD23^{hi}), MZ (IgM^{hi}CD21^{hi}CD23^{lo}), and MZ-P (IgM^{hi}CD21^{hi}CD23^{hi}) CD19⁺ B cells from the indicated mouse strains. **(E)** Confocal microscopic images show the location of mLT⁺CD1d⁺ B cells (yellow) in spleens from the indicated mouse strains. Original magnification, ×20; digitally magnified views of the boxed areas in the top panels are shown in the bottom panels. **(F)** Quantitation of the distribution ratio of mLT⁺CD1d⁺ B cells that were either in the follicles or the MZ (χ^2 test). **(G)** Fluorescence microscopic images of MARCO⁺ MZMs in 2-month-old B6 and B6-*Ltb^{fl/fl} Cd19-Cre* mouse spleens (original magnification, ×4). **(H)** FACS quantitation of the percentage of MZMs (F4/80^{neg}CD11b^{lo}SIGN-R1⁺I-A^{b-}) in spleens from the indicated mouse strains. Data represent the mean ± SEM ($^{\S}P < 0.005$ vs. control B6, Student's *t* test). Results in **D–H** were derived from 4- to 6-month-old mice; *n* = 4–6 mice per group. FO, follicles.

was the downregulation of mechanosensing MKL1 (MRTF-A)/MKL2 (MRTF-B)/serum response factor (SRF) pathways in LTβR-Fc–treated MZMs (Supplemental Table 1 and Supplemental Figure 4A). Changes in the expression of genes in this pathway were further confirmed by quantitative RT-PCR (qRT-PCR) analysis (Supplemental Figure 4B). In contrast, GeneChip and qRT-PCR

analyses indicated normalization of these pathways in BXD2-*Ifnar⁻/⁻* MZMs (Supplemental Table 1 and Supplemental Figure 4), which exhibited sustained interactions with mLT⁺ MZ B cells as compared with BXD2 MZMs.

We showed that in 2-month-old B6 mouse spleens, MKL1 expression was mainly localized in the MZ in a region where
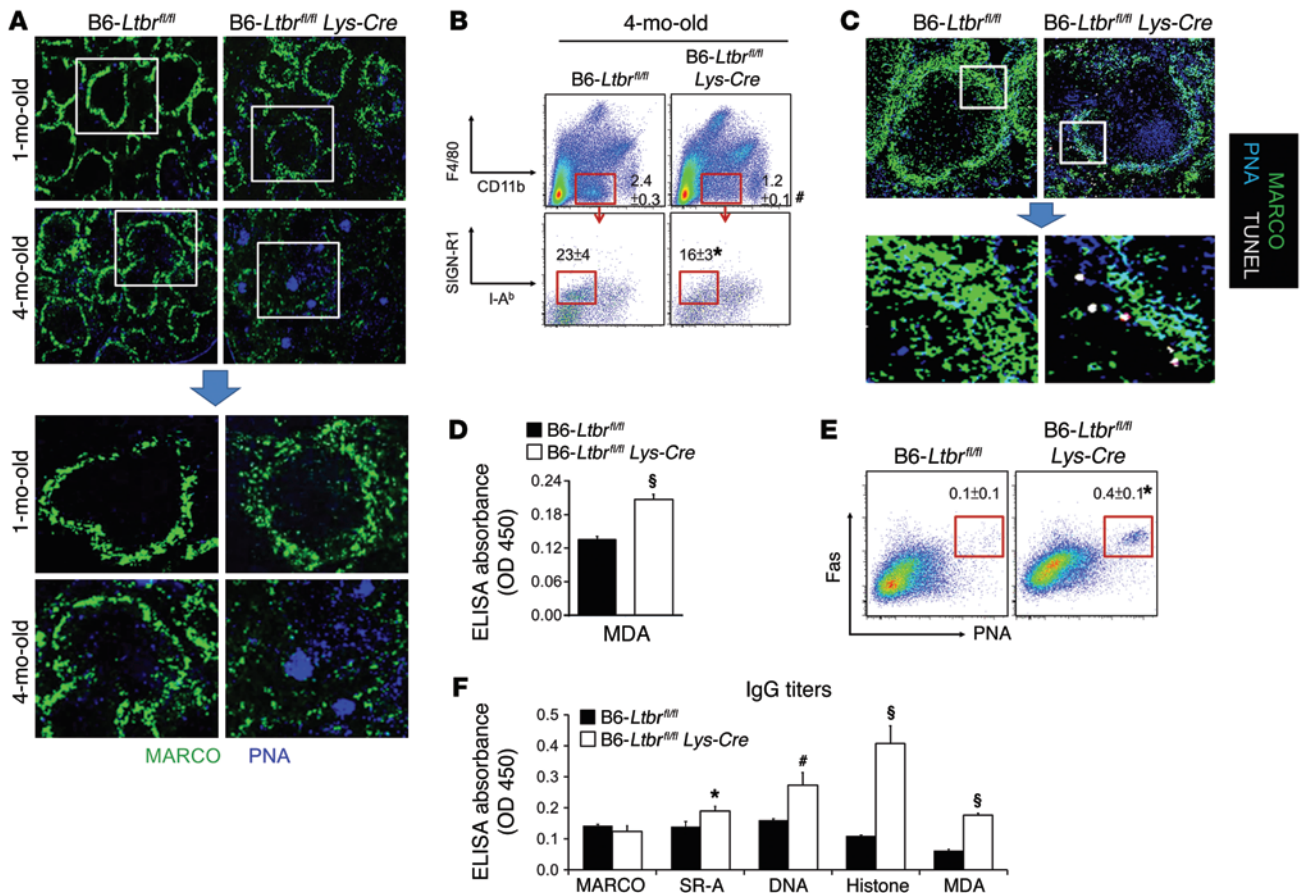
Figure 3. Macrophage-specific deficiency of LTβR is associated with MZM loss and development of spontaneous GCs. (**A**) Fluorescence microscopic images of splenic MARCO+ MZMs and PNA+ GCs in B6-*Ltbr*$^{fl/fl}$ and B6-*Ltbr*$^{fl/fl}$ *Lys-Cre* at the indicated ages. Original magnification, ×4; bottom panels show digitally magnified views of the boxed areas in the top panels. (**B**) FACS quantitation of the percentages of MZMs determined via sequential gating on F4/80^{neg}CD11b^{lo}SIGN-R1+I-A^{b-} in spleens from the indicated mouse strains. (**C**) Confocal microscopic images of splenic MARCO+ MZMs, PNA+ GCs, and TUNEL+ ACs in B6-*Ltbr*$^{fl/fl}$ and B6-*Ltbr*$^{fl/fl}$ *Lys-Cre* mice. Original magnification, ×20; bottom panels are digitally magnified views of the boxed areas in the top panels. (**D**) ELISA analysis of circulating MDA in the indicated mouse strains. (**E**) FACS quantitation of the percentage of PNA+Fas+ GC B cells (CD19+) in spleens from the indicated mouse strains. (**F**) ELISA analysis of serum titers of IgG autoantibody for the indicated autoantigens. Data represent the mean ± SEM (*$P < 0.05$, #$P < 0.01$, §$P < 0.005$ vs. age-matched control mice, Student's *t* test; *n* = 2–3 mice per group for 2 independent experiments; unless otherwise specified, all results were generated using 4-month-old mice).

MARCO+ MZMs were also identified (Figure 4A). Interestingly, MKL1 expression was significantly reduced in the splenic MZ of *Ltb*$^{fl/fl}$ *Cd19-Cre* B6 and BXD2 mice (Figure 4A and Supplemental Figure 5). In contrast, IFNAR deficiency in BXD2 mice restored MKL1 expression levels in the splenic MZ (Figure 4A and Supplemental Figure 5). Consistent with these findings, acute induction of type I IFNs via in vivo administration of CpG or blockade of mLT-LTβR interaction via LTβR-Fc both resulted in a significant reduction in MKL1 expression in MZMs (Figure 4B) and in the percentage of MZMs in B6 mice (Figure 4C), suggesting that either strong IFNAR signaling or reduced mLT signaling abrogated MKL1 expression in MZMs.

LTβR signaling is required for normal cytoskeletal organization in MZMs. MKL1 is localized in the cytoplasm of unstimulated cells by binding to cytoplasmic G-actin (30). Nuclear translocation of MKL1 occurs during mitogenic or mechanical stimulation, which triggers RhoA-mediated actin polymerization, liberating MKL1 from G-actin and exposing a nuclear localization sequence (NLS)

within the actin-binding domain of MKL1 (52). This enables nuclear transport of MKL1 and activation of its downstream target SRF to induce genes related to proper function and survival (26, 29, 53). MZMs isolated from B6, B6-*Ltb*$^{fl/fl}$, and BXD2-*Ifnar*$^{-/-}$ mice exhibited intense, predominantly nuclear expression of MKL1 and F-actin polymerization (Figure 5A). In contrast, both nuclear expression of MKL1 and F-actin polymerization were significantly reduced in MZMs isolated from B6-*Ltb*$^{fl/fl}$ *Cd19-Cre*, B6-*Ltbr*$^{fl/fl}$ *Lys-Cre*, and BXD2 mice (Figure 5A and Supplemental Figure 6).

To determine whether the absence of LTβR signaling only in hematopoietic cells, especially myeloid lineage cells, could affect MZM repopulation and maintenance, MKL1 expression, and F-actin polymerization, a mixed BM transfer experiment was carried out, in which BM from WT CD45.1 mice was transferred with BM from either WT CD45.2 mice or *Ltbr*$^{fl/fl}$ *Lys-Cre* CD45.2 mice into B6-*Rag1*$^{-/-}$ mice (Supplemental Figure 7A). Four months after BM reconstitution, there was an age-related loss of *Ltbr*$^{fl/fl}$ *Lys-Cre* BM–derived MZMs in the spleens of recipient mice, although the
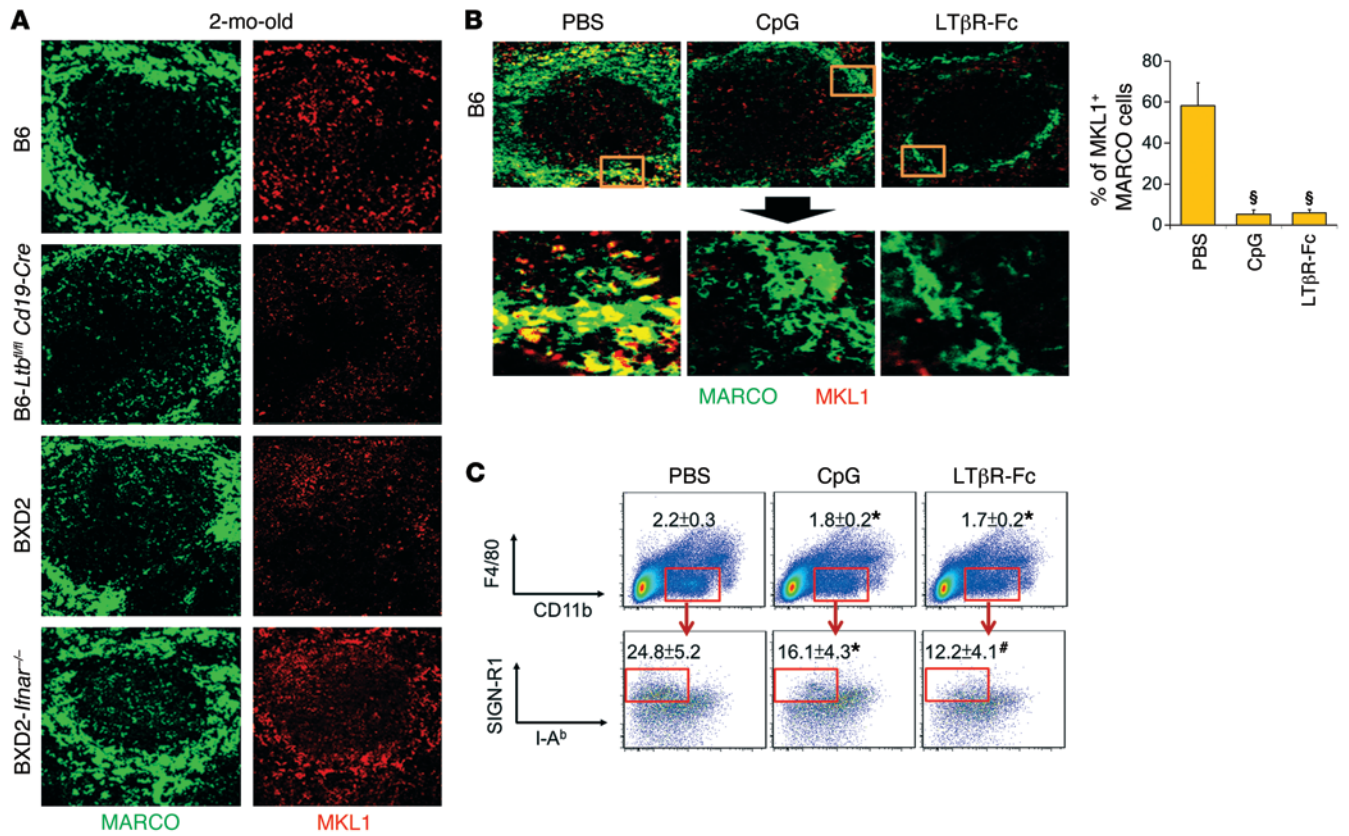
Figure 4. Defective LTβR signaling is associated with decreased expression of MKL1 in MZMs. (**A**) Representative confocal microscopic images of splenic MARCO (green) or MKL1 (red) from the indicated mouse strains. Original magnification, ×20. (**B**) Right: Confocal images show colocalization of MKL1 with MARCO⁺ MZMs in 2-month-old B6 mice treated with PBS, CpG, or LTβR-Fc 30 hours before the analysis. Original magnification, ×20; bottom panels show digitally magnified views of the boxed areas in the top panels. Left: Quantitation of the percentage of MARCO⁺ cells that also showed positive staining for MKL1 (≥10 randomly chosen areas per follicle for 3–5 follicles). (**C**) FACS quantitation of the percentage of MZMs (F4/80^neg^CD11b^lo^SIGN-R1⁺I-A^b−) in the spleens of B6 mice with the indicated treatment. Data represent the mean ± SEM, and all images are from a representative splenic region or splenic follicle from each group (*$P < 0.05$, #$P < 0.01$, §$P < 0.005$ vs. B6, PBS-treated B6, Student's t test; $n = 2$–3 mice per group for 2 independent experiments).

repopulation of WT and *Ltbr^fl/fl^ Lys-Cre* MZMs 1 month after the chimeric transfer was comparable (Supplemental Figure 7B). Despite the small number of events that could be collected, ImageStream cytometric analysis further showed lower expression of MKL1 and defective F-actin polymerization in B6-*Ltbr^fl/fl^ Lys-Cre* BM–derived MZMs in the spleens of recipient mice 4 months after BM transfer (Figure 5B and Supplemental Figure 7C). The results suggest that LTβR signaling in MZMs may act through MKL1 for maintenance, but not recruitment or early development, of MZMs in the MZ.

MKL1 deficiency leads to gradual loss of MZMs. It was shown previously that macrophage phagocytic function is impaired when SRF expression is suppressed (54). B cell–specific deletion of SRF also leads to complete deficiency of MZ, but not follicular, B cells, suggesting that MKL1-SRF–mediated cell elasticity is essential for the maintenance of MZ integrity (55). We analyzed B6-*Mkl1^-/-^* mice to directly show that an MKL1 deficiency affects MZM numbers and function. Consistent with the results obtained in older *Ltbr^fl/fl^ Lys-Cre* mice, there was a dramatic reduction in MZMs in 8-month-old B6-*Mkl1^-/-^* mice compared with those in age-matched WT controls (Figure 6A). F-actin polymerization, as shown by phalloidin staining, was reduced in the cytoplasmic rim of MZMs isolated from 4-month-old B6-*Mkl1^-/-^* mice (Figure 6B).

Consistent with our results in *Ltbr^fl/fl^ Lys-Cre* B6 mice, the percentage and number of MZMs were gradually reduced in the spleens of B6-*Mkl1^-/-^* mice from 1 month to 4 months of age (Figure 6, C and D). These results further support the critical role of the LTβR/MKL1 axis in maintaining MZMs in the MZ.

To compare the phenotype of *Mkl1^+/+^* MZMs with that of *Mkl1^-/-^* MZMs in the same microenvironment, we generated mixed BM chimeric mice by transferring a 1:1 ratio of BM derived from CD45.2 WT plus CD45.1 WT mice or CD45.2 B6-*Mkl1^-/-^* plus B6 CD45.1 WT mice into B6-*Rag1^-/-^* mice (Supplemental Figure 8A). We found an age-associated reduction in the percentage of MZMs derived from CD45.2 B6-*Mkl1^-/-^* mice compared with the percentage of CD45.1 B6-MKL1⁺ MZMs in the same splenic microenvironment (Supplemental Figure 8B), as well as defective F-actin polymerization in the cytoplasmic rim of MKL1-deficient MZMs (Figure 6E and Supplemental Figure 8C). The results suggest that an intrinsic MKL1 deficiency can gradually promote mechanosensing defects in MZMs.

As mechanosensing signaling has been implicated in the normal phagocytic function of macrophages (23, 24, 28), we tested the possibility that the MKL1 pathway affects the AC clearance function of MZMs. For this experiment, CFSE-labeled apoptotic
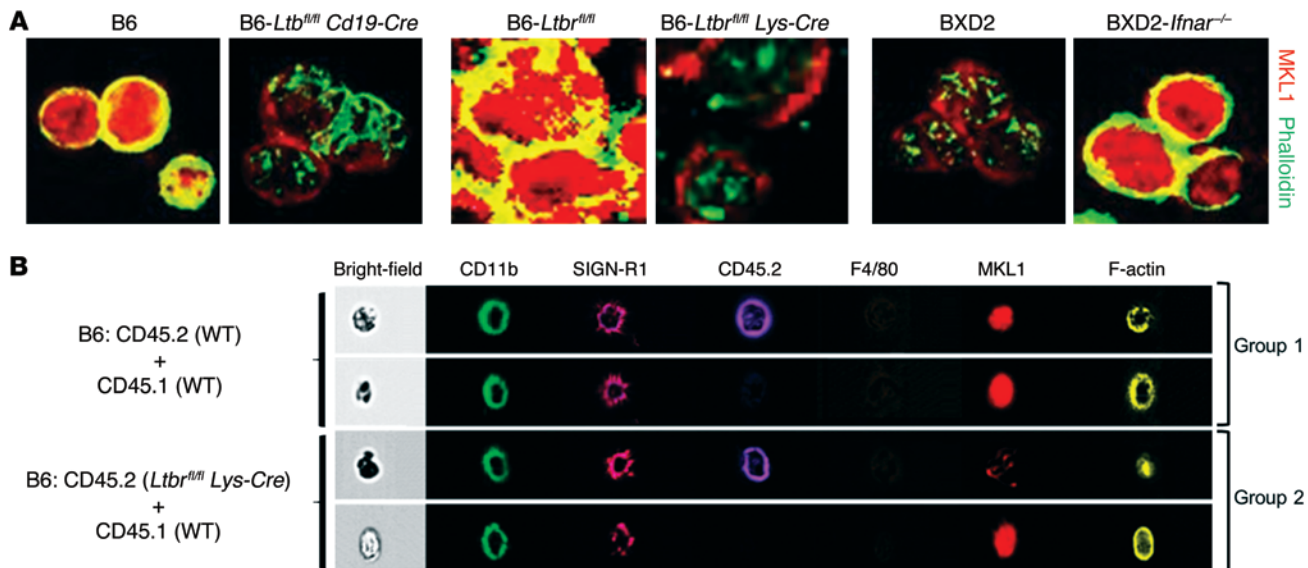
Figure 5. Defective LTβR signaling is associated with decreased MKL1 expression and F-actin polymerization in MZMs. (**A**) Representative confocal microscopic images of sorted splenic MZMs from the indicated mouse strains for expression and subcellular localization of MKL1 (red) and phalloidin-counterstained F-actin (green). Original magnification, ×63. (**B**) Representative ImageStream photomicrographs of MKL1 expression and F-actin polymerization in splenic MZMs (CD11b^{lo}SIGN-R1^{+}F4/80^{neg}) from recipient B6-*Rag1*^{−/−} mice 4 months after transfer of equal numbers of BM cells from the indicated mice. Data represent the mean ± SEM, and all images are of representative cells from each group (*n* = 2–3 mice per group for 2 independent experiments).

thymocytes from B6 mice were administered to 1.5-month-old B6 and B6-*Mkl1*^{−/−} mice, prior to the loss of MZMs in B6-*Mkl1*^{−/−} mice. Residual uncleared ACs in the splenic MZ were visualized by confocal imaging analysis. Although B6 MZMs rapidly internalized ACs within 15 minutes, there was a markedly lower uptake of ACs in MZMs from B6-*Mkl1*^{−/−} mice at both the 15- and 30-minute time points (Figure 6F). Consistent with these observations, the AC phagocytic function of BM-derived macrophages from B6-*Mkl1*^{−/−} mice was considerably impaired compared with that observed in BM-derived macrophages derived from normal B6 mice (Figure 6G). In vitro treatment of BM-derived macrophages from B6 mice with CCG-100602, an SRF inhibitor, resulted in a significant decrease in AC uptake, suggesting that a transient impairment in this pathway is sufficient to interfere with the AC clearance function of macrophages (Figure 6H).

Decreased MKL1 in B6.TC mice and in patients with SLE. We have analyzed the spleens of lupus-prone B6.TC mice and of patients with SLE, which also exhibited aggregation of pDCs and loss of MARCO[+] MZMs in the MZ (Figure 1 and ref. 42). Consistent with the findings in BXD2 mouse spleens, we observed an age-related follicular migration of mLT^{+} cells (Figure 7A) and a significant loss of MKL1 expression in MARCO[+] MZMs (Figure 7B) in spleens from older B6.TC mice. Importantly, consistent with findings in both lupus mouse strains, a significantly reduced number of perifollicular CD1c^{+} MZ B cells was associated with visible follicular translocation of CD1c^{+} MZ B cells (ref. 56 and Figure 7C) and loss of MKL1 expression in the perifollicular region (Figure 7D) in the spleens of patients with SLE. These results suggest that the combined features described above can be identified in the spleens of patients with SLE.

MKL1/SRF defects enhance autoimmunity. A key question is whether a deficiency of MKL1 by itself is sufficient to promote auto-

immunity in otherwise normal mice. There was a 2-fold increase in the percentage of PNA[+]Fas[+] GC B cells in the spleens of 4-month-old B6-*Mkl1*^{−/−} mice compared with that observed in B6 mouse spleens (Figure 8A). Circulating levels of autoantibodies were significantly elevated in 4-month-old B6-*Mkl1*^{−/−} mice compared with those detected in age-matched B6 mice. Interestingly, these autoantibodies were less prominent compared with those that developed in age-matched BXD2 mice (Figure 8B), which exhibit additional immune dysregulation in the GCs (17, 34). However, at 8 months of age, B6-*Mkl1*^{−/−} mice developed severe IgG glomerulonephritis, as shown by significantly elevated IgG deposition in glomeruli (Figure 8C).

The SRF pathway may be regulated via signaling of MKL1 and MKL2 (26, 54, 57), and MKL1 signaling may be important to maintain other hematopoietic cells (27). We thus administered CCG-100602 (58) using a liposome-based delivery system to induce selective uptake by MZMs (2) in both B6 and BXD2 mice. MZM numbers were decreased in both B6 and BXD2 mice 4 weeks after CCG-100602–liposome treatment compared with those detected in control PBS-liposome–treated groups (Figure 8, D and E). In association with the reduction of MZMs in CCG-100602–liposome–treated mice, there was significantly enhanced GC formation (Figure 8F) in the spleen, elevated autoantibody serum titers (Figure 8G), and statistically significantly increased IgG deposition — especially in BXD2 mice — in the glomeruli (Supplemental Figure 9) compared with PBS-liposome–treated mice, suggesting that MZM-targeted disruption of the SRF pathway initiated and further exacerbated MZM loss and autoantibody development in both normal and autoimmune mice.

Discussion

Expression of type I IFN signature genes is a well-established characteristic of SLE. The pathogenic role of type I IFNs has been
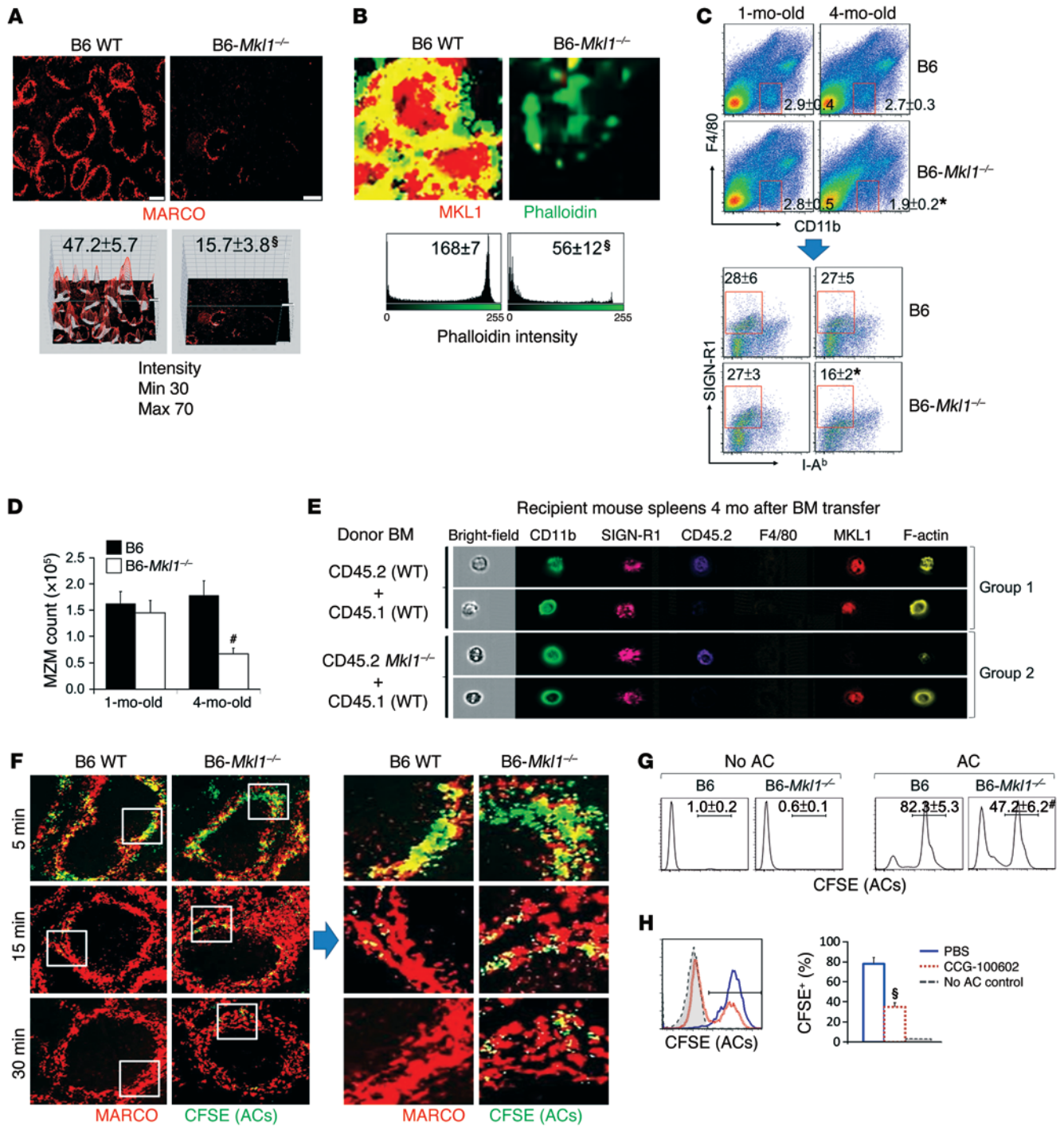
Figure 6. Deficiency of MKL1 is associated with defective F-actin polymerization and reduced AC clearance of MZMs. (**A**) Representative fluorescence photomicrographs (top) and ImageJ 3D intensity plots (bottom) of splenic MARCO+ MZMs in 8-month-old mice (original magnification, ×4). Maximal and minimal intensity scales set for the plots are shown on the left. (**B**–**D**) Spleens of B6 and B6-$Mkl1^{-/-}$ mice were analyzed for (**B**) MKL1 and F-actin polymerization (phalloidin+) in FACS-sorted MZMs, (**C**) frequency of F4/80^{neg}CD11b^{lo}SIGN-R1+I-A^{b-} MZMs (red boxed areas), and (**D**) quantitation of total MZM cells. (**E**) Representative ImageStream photomicrographs of MKL1 expression and F-actin polymerization in splenic MZMs (CD11b^{lo}SIGN-R1+F4/80^{neg}) from recipient B6-$Rag1^{-/-}$ mice. (**F**) Confocal microscopic images of AC clearance in the indicated mouse spleens following transfer of CFSE-labeled ACs (green) at the indicated times. Original magnification, ×20; digitally magnified views of the boxed areas are shown on the right. (**G**) FACS analysis of in vitro CFSE+ AC uptake by BM-derived macrophages 30 minutes after incubation with ACs. (**H**) FACS analysis of the effects of CCG-100602 on uptake of CFSE+ ACs by BM-derived macrophages from B6 mice. Bar graph shows the percentage of macrophages that were positive for CFSE+ ACs. Data represent the mean ± SEM. Results are from 3 to 5 randomly chosen follicles (**A**) or 20 randomly chosen cells (**B**) (n = 4–6; *P < 0.05, #P < 0.01, and §P < 0.005, compared with results from age-matched B6 mice, PBS-treated controls, or between the indicated groups, Student's t test).
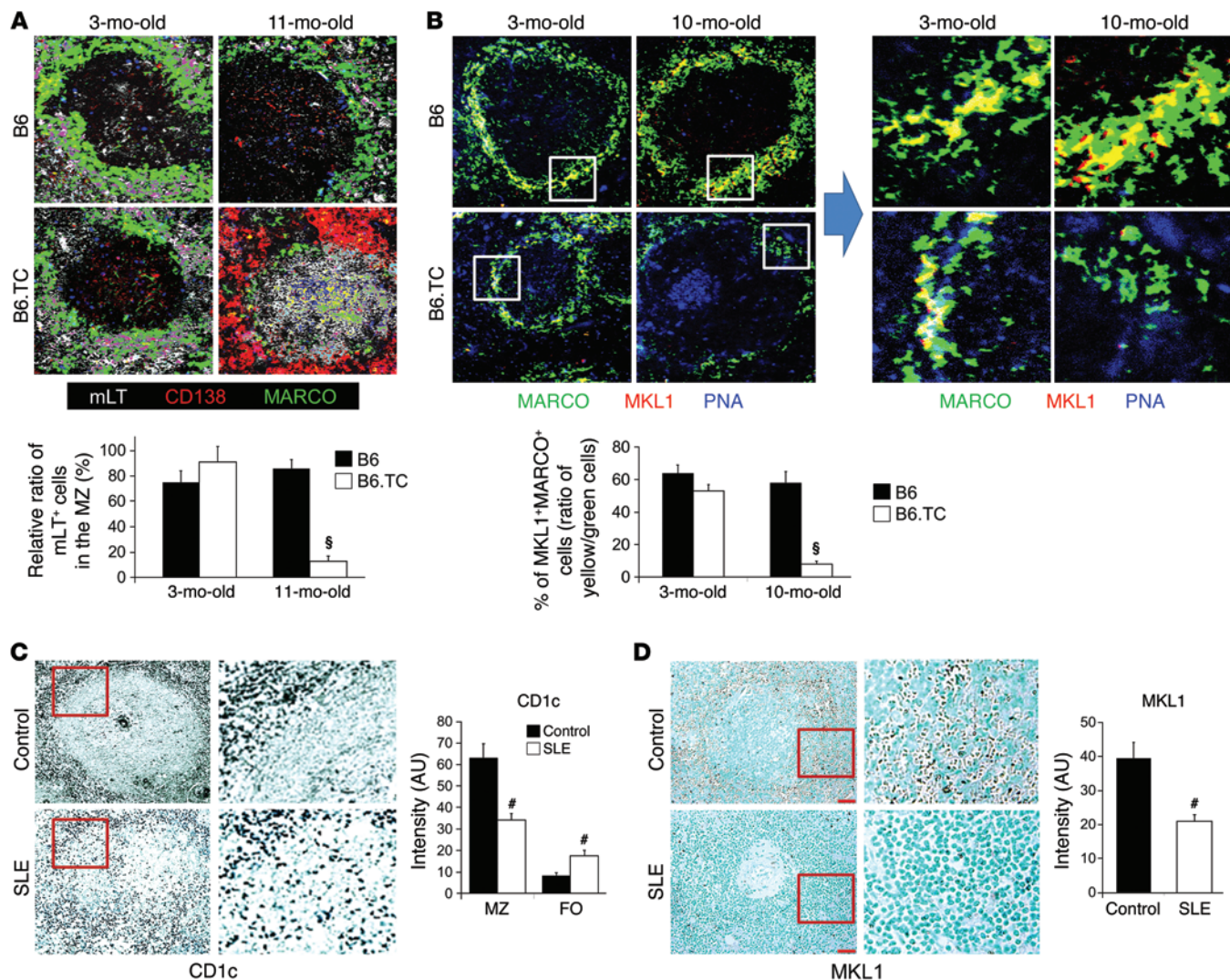
Figure 7. Follicular translocation of MZ B cells and decreased expression of MKL1 in lupus B6.TC mouse and human SLE spleens. (**A** and **B**) Spleens obtained from B6 and B6.TC mice at the indicated ages were analyzed. (**A**) Confocal microscopic images of mLT, CD138, and MARCO for a representative splenic follicle from each group. Original magnification, ×20. (**B**) Confocal microscopic images of MARCO, PNA, and MKL1 for a representative splenic follicle from each group. Original magnification, ×20. Boxed areas in the left 4 panels are shown digitally magnified in the right 4 panels. Bar graphs show quantitation of the relative percentage of mLT⁺ cells that were in the MZ (**A**) or the percentage of MARCO⁺ cells that were also MKL1⁺ (**B**). At least 10 randomly chosen areas were counted per follicle, and 3–5 follicles were analyzed for each spleen. All data represent the mean ± SEM ($^{\#}P < 0.01$, $^{\S}P < 0.005$ vs. B6; $n = 3$–4 mice from each group). (**C** and **D**) IHC staining of CD1c⁺ MZ B cells (**C**) and MKL1 (**D**) in paraffin-embedded spleen sections derived from normal individuals ($n = 6$) and patients with SLE ($n = 5$). Original magnification, ×20. Boxed areas are shown digitally magnified on the right. ImageJ intensity quantitation of 10 randomly selected splenic perifollicular regions per section is shown on the right. Data represent the mean ± SEM ($^{\#}P < 0.01$, $^{\S}P < 0.005$ vs. B6 mice or non-SLE controls, Student's t test).

mainly implicated in directly stimulating adaptive autoimmune responses (43), and the increased expression of type I IFNs was considered a downstream consequence of AC clearance defects (1). The new findings presented here suggest an alternative pathogenic role of type I IFNs in lupus, whereby type I IFNs perpetuate AC clearance defects and promote the loss of immune tolerance to AC-Ags in SLE by promoting a defective LTβR/MKL1 axis in MZMs. Our results suggest that although type I IFNs do not directly act on MZMs, they dissipate MZMs via disruption of the interactions between MZ B cells and MZMs. This interferes with the mLT/LTβR signaling that is associated with this cellular interaction. Our results therefore provide what we believe to be a new

model of lupus based on the concept that type I IFNs interfere with key MZ B cell–MZM crosstalk in the perifollicular structure by promoting follicular migration of mLT⁺ MZ B cells (Supplemental Figure 10). In this model, the definition of an autoimmune pathogenic cell is based on the cell's anatomic location, in that type I IFNs shift the innate-like mLT⁺ MZ B cells from their tolerogenic site in the MZ, where they are essential for maintenance of MZMs to clear ACs, to an immunogenic site near the FDC network, where they can stimulate a GC response (48).

At the structural and molecular levels, we have identified that pDCs are increased in the splenic MZ of both lupus-prone BXD2 (20, 21) and B6.TC mice (42) and that both strains exhibit follicular
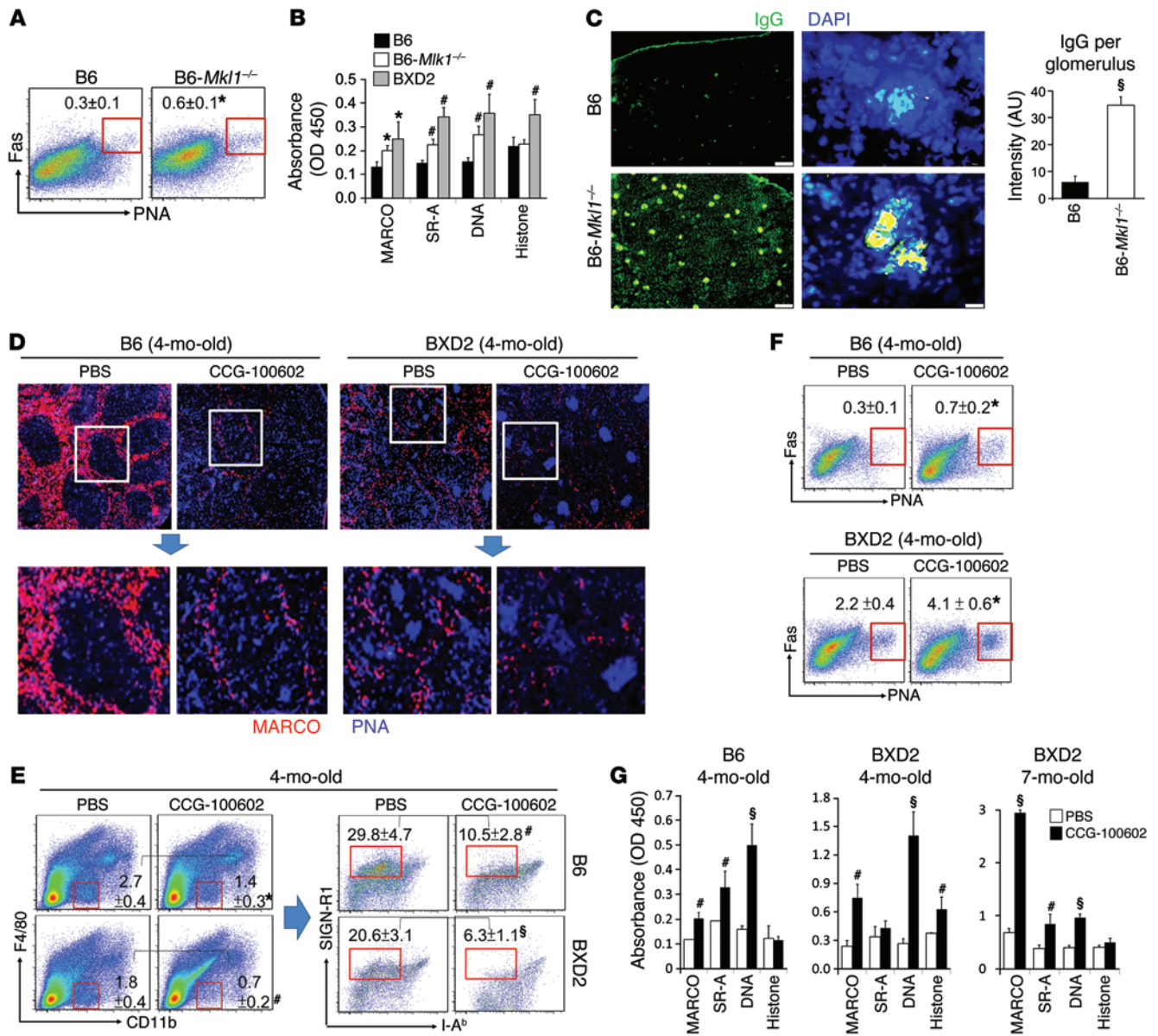
Figure 8. Disruption of the MKL1/SRF mechanosensing pathway leads to autoantibody production. (**A**) FACS analysis of GC B cells (Fas⁺PNA⁺ gated within CD19⁺ B cells) in spleens from 4-month-old B6 and B6-*Mkl1*⁻/⁻ mice. (**B**) ELISA analysis of IgG autoantibodies in the serum of 4-month-old mice. (**C**) Fluorescence microscopic images and ImageJ quantitation of the intensity of IgG staining in the kidneys of 8-month-old B6 WT and B6-*Mkl1*⁻/⁻ mice. At least 20 glomeruli were quantitated per kidney. Original magnification, ×4 (left panels), ×40 (right panels). (**D**–**G**) B6 and BXD2 mice (3- or 6-month-old) were administered either liposome-PBS or liposome-CCG100602. Mice were sacrificed 4 weeks later at the indicated ages. (**D**) Fluorescence microscopic images of MARCO⁺ MZMs (red) and PNA⁺ GCs (blue) in the spleen. Original magnification, ×4; bottom panels are digitally magnified views of the boxed areas in the top panels. (**E**) FACS analysis of MZMs in spleens. MZMs were quantitated via sequential gating on F4/80 and CD11b (F4/80^{neg}CD11b^{lo}) (left), followed by SIGN-R1 versus I-A^b (SIGN-R1⁺I-A^{b-}) gating (right). (**F**) FACS analysis of splenic PNA⁺Fas⁺ GC CD19⁺ B cells. (**G**) ELISA analysis of IgG autoantibodies against the indicated Ags in serum from mice. Data represent the mean ± SEM (n ≥ 6 mice/group; *P < 0.05, #P < 0.01, §P < 0.005 vs. B6 or PBS-liposome–treated controls, Student's t test).

migration of mLT⁺ cells and decreased MKL1 expression in MZMs. A strikingly similar finding was identified in the spleens of patients with SLE. In mice, we found that IFNAR deficiency corrected MZM cytoskeletal defects and rescued MZMs in BXD2 mice. In contrast, local deficiency of LTβR or MKL1 promoted such defects. Consistent with our findings, it was reported that in BXSB mice, abnormally elevated TLR7 is associated with loss of MZ B cells and that elimination of pDCs also reversed this phenotype (3). Collectively, these results

suggest that under conditions of chronically elevated type I IFN levels, as seen in BXD2 mice and other lupus-prone mice, the clearance of AC-Ags is gradually compromised as a result of MZM defects.

The present studies also underscore the significance of cellular elasticity in controlling immune activation and tolerogenic responses (59, 60). Mechanical receptor activity and actin cytoskeletal dynamics are regulated through key molecules such as MKL1 to activate the signaling cascades that are necessary to control the

movement and protrusion of extracellular membrane and thus exhibit an important function to integrate immune responses (53). Alterations in the MKL1/SRF axis can lead to defects in nuclear translocation and function of stress fiber actin cytoskeleton, leading to changes in cell morphology, function, and, eventually, cell fate (59). This is consistent with previous findings that members of the Rho family GTPases are important mediators of macrophage recruitment and function in both humans and mice (61). Thus, in different mouse models of lupus and potentially in patients with SLE, aberrant mechanosensing signaling in phagocytic macrophages might occur by the effects of type I IFN or by an intrinsic genetic defect. In either case, we believe this constitutes an important central defect underlying the gradual changes in MZMs, whereby they lose their phagocytic function and survival in the important niche in the spleen, thus leading to defective clearance of ACs in lupus (Supplemental Figure 10).

Potential limitations of the immunohistological studies of the spleen from lupus and unaffected subjects are that the depletion of MZMs and MZ B cells may result from other factors associated with the disease, such as elevated anti-MARCO and class A scavenger receptor (SR-A) antibodies, which has been reported in patients with SLE (62). Additionally, the depletion of MZMs and B cells in patients with SLE could be due to treatment with cytotoxic therapies that may deplete these cells or MZMs. Therefore, additional studies of human SLE spleens would be required to confirm the present results. Studies using ImageStream analysis are limited by the small number of cells that can be analyzed and the small percentage of MZMs in BM chimeric mice.

In summary, the present work suggests a novel pathogenic role for type I IFN–mediated follicular shuttling of innate-like mLT⁺ B cells in systemic autoimmunity. Furthermore, alterations in the mechanosensing properties of MZMs responsible for phagocytosis of apoptotic debris represent a risk factor for loss of immune tolerance to AC-Ags which, combined with other risk factors, can ultimately lead to development of autoreactive GCs (2, 17, 21, 36). Suppression of type I IFNs or their signals may act through restoration of MZMs to ameliorate the severity of SLE. Reagents that can specifically restore the mechanosensing function of SRF and MKL1 in MZMs should offer a novel strategy to prevent the onset and progression of lupus.

Methods

Mice. WT C57BL/6 (B6), B6-CD45.1, B6-*Rag1*⁻/⁻, B6-GFP⁺ transgenic, and BXD2 recombinant inbred mice were obtained from The Jackson Laboratory. B6-*Ifnar*⁻/⁻ mice were provided by Jocelyn Demengeot (Instituto Gulbenkian de Ciência, Oeiras, Portugal); *Ltbr*^fl/fl^ *Lys-Cre* mice were generated by Yang-Xin Fu (University of Chicago); and *Ltb*^fl/fl^ *Cd19-Cre* mice were obtained from Louis B. Justement (UAB). *Mkl1*⁻/⁻ mice were provided by Stephan W. Morris (Insight Genetics Inc.), and B6.TC mice were generated by Laurence M. Morel (University of Florida). B6-*Rag1*⁻/⁻ and B6 GFP⁺ transgenic and B6-*Ifnar*⁻/⁻ mice were backcrossed with BXD2 mice for 10 generations to generate BXD2-*Rag1*⁻/⁻, BXD2-GFP⁺ transgenic, and BXD2-*Ifnar*⁻/⁻ mice, respectively. All mice were maintained under specific pathogen–free conditions at the animal facilities of the UAB.

In vivo treatment. For lymphotoxin blockade, mice were injected i.v. with 25 μg sLTβR-Fc (generated by Yang-Xin Fu, University of Chi-

cago) (63). For MZ B cell depletion, 1-month-old B6 and BXD2 mice were injected i.v. with 200 μg neutralizing anti-DLL1 mAb (generated by Hideo Yagita, Juntendo University School of Medicine) (44) every week for 1 month. Nonspecific hamster IgG isotypes were injected as a negative control.

CCG-100602 treatment. CCG-100602–liposome (5 ml liposome formulation composed of 65:25:10 molar ratios of phosphatidylcholine (PC)/cholesterol/CCG-100602, sized to 1 μm) was made by Encapusla NanoSciences. For CCG-100602–liposome in vivo treatment, mice were administered i.v. CCG-100602–liposome (100 μg/mouse) or PBS-liposome every other day for 4 weeks. For CCG-100602 in vitro treatment, polarized macrophages were cultured with or without CCG-100602 (1 μmol/l) for 1 hour before the addition of ACs.

BM transplantation. BM cells were harvested from WT C57BL/6 (B6), B6-CD45.1, B6-CD45.2-*Ltbr*^fl/fl^ *Lys-Cre*, B6-CD45.2-*Mkl1*⁻/⁻, BXD2, GFP⁺ transgenic BXD2, and GFP⁻ BXD2-*Ifnar*⁻/⁻ mice. BM cells (total of 2 × 10⁷) from the indicated donors were transferred or mixed at a 1:1 ratio and injected i.v. into the recipient mice immediately after irradiation. Mice were kept on sulfatrim water for 14 days and sacrificed 1 month or 4 months after irradiation.

Apoptosis induction and in vitro and in vivo AC clearance assay. For the generation of ACs, thymocytes collected from 8-week-old female B6 mice were cultured with 1 μM dexamethasone (D4902-100MG; Sigma-Aldrich) for 6 hours at 37°C in RPMI 1640 media plus 1% FBS (MT-17-105-CV; Fisher Scientific). BM-derived macrophages were polarized by culturing BM cells in RPMI medium with M-CSF (10 ng/ml) for 7 days. For in vitro AC clearance assays, 5 × 10⁶ BM-derived macrophages were cultured with 1 × 10⁶ Vybrant CFDA SE Cell Tracer–labeled ACs (V12883; Life Technologies) for 30 minutes. For in vivo administration of ACs, each mouse was injected i.v. with 2 × 10⁷ apoptotic thymocytes and sacrificed at 5-, 15-, and 30-minute time points.

Type I IFN induction in vivo. For in vivo induction of type I IFNs, 5 μg CpG-A (HC4037; Hycult Biotech) was mixed with 50 μl PBS, while in another reaction tube, 30 μl DOTAP (11811177001; Roche) was mixed with 70 μl PBS. The CpG solution was then mixed with the DOTAP solution, incubated at room temperature for 15 minutes prior to i.v. administration in the tail.

Type I IFN RNA quantitation. Expression levels of the type I IFN isoforms *Ifna1*, *Ifna4*, *Ifna7*, *Ifna9*, *Ifna11*, and *Ifnb* in peripheral blood were determined using a previously described qRT-PCR method (21). The qRT-PCR mixtures contained SYBR Green PCR Master Mix (Bio-Rad) with the following primers: *Ifna1*, forward: 5′-AGTGAGCTGACC-CAGCAGAT-3′, reverse: 5′-GGTGGAGGTCATTGCAGAAT-3′; *Ifna4*, forward: 5′-TCTGCAATGACCTCCATCAG-3′, reverse: 5′-TATGTCCT-CACAGCCAGCAG-3′; *Ifna7*, forward: 5′-ATGGATCCCTCCTAGACT-CATT-3′, reverse: 5′-CAACTTGGCTGAGGAAGACA-3′; *Ifna9*, forward: 5′-TGATGGTCTTGGTGGTGATAAG-3′, reverse: 5′-GTGC-CAGGAGTGTCAAGATT-3′; *Ifna11*, forward: 5′-CCCAGCAGATCTT-GAACCTC-3′, reverse: 5′-GGTGGAGGTCATTGCAGAAT-3′; *Ifnb*, forward: 5′-CTCCACCACAGCCCTCTC-3′, reverse: 5′-CATCTTCTC-CGTCATCTCCATAG-3′; and *Gapdh*, forward: 5′-ACCACAGTCCAT-GCCATCAC-3′, reverse: 5′-TCCACCACCCTGTTGCTGTA-3′.

qRT-PCR analysis for GeneChip analysis validation. Expression levels of *Prg2*, *Prg3*, *Prtn3*, *Cldn15*, *Slip1*, *Epx*, *Cpa3*, and *Ets1* in isolated MZMs from the indicated mouse strains as shown in Supplemental Figure 4B were determined using the qRT-PCR method described above with the following primers: *Ets1*, forward: 5′-TCCTGCAGAAAGAG-

GATGTG-3′, reverse: 5′-CTGAGGGAGGAACACACTGA-3′; *Prg2*, forward: 5′-GGGTTGATGGAAGTTCTTGG-3′, reverse: 5′-CAGT-GGCCTCCTTGAGTACA-3′; *Prg3*, forward: 5′-CTTGCTTCCGTC-CACAGTTA-3′, reverse: 5′-ACTTCTTCCAGAACCATCCC-3′; *Prtn3*, forward: 5′-CTTCTCCTCCAGCTAAACCG-3′, reverse: 5′-GACAGAG-TCTGGTCCTGCTG-3′; *Cldn15*, forward: 5′-CAGGGACCCTCCA-CATACTT-3′, reverse: 5′-GGCCCAGTTCATACTTGGTT-3′; *Slip1*, forward: 5′-ATGTGAGCCTGATCCCTGA-3′, reverse: 5′-TGGGAG-CAGGGAAGTAGTTT-3′; *Epx*, forward: 5′-TCAGCAAGTGAGAAG-GATCG-3′, reverse: 5′-AGGCATTGTATCCTGGAAGG-3′; *Slip1*, forward: 5′-ATGTGAGCCTGATCCCTGA-3′, reverse: 5′-TGGGAG-CAGGGAAGTAGTTT-3′; and *Cpa3*, forward: 5′-TCATGGACACAG-GATCGAAT-3′, reverse: 5′-ATGGTTTGTTGGTGTTTGGA-3′.

Histology of frozen sections. Spleens were embedded in OCT tissue media (Tissue-Tek) and frozen on dry ice. Frozen sections (7 μm thickness) were fixed to slides in ice-cold acetone for 15 minutes and air dried for 30 seconds. The sections were blocked with 10% horse serum for 30 minutes at room temperature and then stained for 30 minutes at room temperature in a humidified chamber with fluorescently labeled antibody cocktails and biotinylated PNA (B-1075; Vector Laboratories). The following conjugations with Alexa Fluor dyes (Life Technologies) were applied according to the manufacturer's instructions: IgM (catalog A-21426; Life Technologies); anti-MARCO (clone ED31, catalog MCA1849; AbD Serotec); anti–SIGN-R1 (clone LWC06; eBioscience); anti-CD138 (clone ab60199; Abcam); anti-CD21/CD35 (clone 8D9; eBioscience); anti-CD1d (clone 1B1; eBioscience); anti-PDCA1 (clone 129c; eBioscience); anti-VCAM1 (clone 429; eBioscience); anti-CD23 (catalog sc-9152; Santa Cruz Biotechnology Inc.); and anti-MKL1 (catalog ab49311; Abcam). Biotinylated PNA was detected using streptavidin–Alexa Fluor 350 (catalog S-11249; Life Technologies). Lymphotoxin β on B cells was stained with sLTβR-Fc first and further detected by biotin-conjugated goat anti-human Fc antibody (catalog 13-4998; eBioscience) and streptavidin–Alexa Fluor 488 (catalog A-32361; Life Technologies). F-actin was stained with Biotin XX phalloidin (catalog B7474; Life Technologies). In situ quantitation was performed using ImageJ software (NIH) (48).

Histology of paraffin-embedded tissue sections. Deidentified cadaver paraffin-embedded splenic tissue sections were obtained from the UAB Tissue Procurement Shared Facility. Following heat-induced epitope retrieval, endogenous peroxidase activity was suppressed by incubating the slides in 3% H_2O_2 for 5 minutes. Sections were incubated in PBE buffer (PBS containing 1% BSA, 1 mM EDTA, and 0.15 mM NaN3, pH 7.6) with 1% goat serum for 20 minutes to reduce nonspecific staining. The sections were then incubated overnight with the purified rabbit anti-human MARCO (catalog bs-2659R; Bioss Antibodies); purified rabbit anti-human MKL1 (catalog ab49311; Abcam); mouse anti-human CD1c (catalog 331504; BioLegend); or mouse anti-human pDCA1 (clone 26F8; eBioscience), separately diluted in PBE buffer. The HRP-conjugated goat anti-rabbit or goat anti-mouse secondary antibody was applied for 20 minutes. The DAB substrate reagent (catalog 34001; Life technologies) was prepared immediately before use and applied for 7 minutes. The stained sections were lightly counterstained with hematoxylin before mounting. In all cases, negative controls, consisting of incubations without the primary antibody, were included in the analyses. In situ quantitation was performed using ImageJ software (48).

Flow cytometry. Cell suspensions were prepared from spleens and stained at 4°C in PBS containing 2% FCS and 0.5% EDTA after FcγRII/III blocking. Surface staining was performed with the following antibodies: anti-CD11c (clone N418); anti-CD11b (clone M1/70); anti-MHC class II I-A^b (clone AF6-120.1); anti-CD19 (clone 1D3); anti-PDCA1 (clone 129c); anti-CD23 (clone B3B4); anti-CD21/35 (clone 8D9); anti-IgM (clone 121-15F9); anti-FAS (clone 15A7); anti-F4/80 (clone BM8); and anti–SIGN-R1 (clone 22D1). All antibodies were from either eBioscience or BioLegend, except biotinylated peanut agglutinin (PNA), which was from Vector Laboratories, and anti-IFNα (clone 32100-1), which was from PBL and was further detected by fluorescence-conjugated donkey anti-rabbit IgG (Life Technologies). Dead cells were excluded using Fixable Viability Dye staining (Life Technologies).

ImageStream analysis. Images were obtained with a ×100 oil immersion objective lens (numerical aperture 1.45) and processed using IDEAS, version 6.1 software (Amnis, EMD Millipore). MZMs were gated as CD11b^{lo}F4/80$^-$SIGN-R1$^+$ cells, and histograms of the cytoplasmic rim expression of actin and MKL1 expression in CD45.1$^+$ versus CD45.2$^+$ cells were further plotted. A total of 10,000 splenic cells were collected and analyzed in each sample.

Autoantibody detection. Assays for serum autoantibodies were carried out as described previously (17). Multiple antigenic targets were analyzed due to the development of polyreactive pathogenic autoantibodies in BXD2 mice (34). Immulon II plates (Dynatech) precoated with BSA were coated individually with 50 μg/ml calf thymus DNA (Sigma-Aldrich), 25 μg/ml MDA (Cell Biolabs), 25 μg/ml recombinant mouse MARCO, or 25 μg/ml recombinant mouse SR-AI/MSR1 (R&D Systems). The serum was diluted and assayed for autoantigen reactivity against the plates described above by incubation for 2 hours at room temperature. Bound IgG was detected with a goat polyclonal HRP–anti-mouse IgG detection antibody (catalog 1030-50; SouthernBiotech) and visualized at 450 nm using a tetramethylbenzidine (TMB) substrate (Sigma-Aldrich).

Detection of MDA. Immulon II plates precoated with BSA were coated with 50 μg/ml goat polyclonal anti-MDA antibody (catalog ab27644; Abcam). Following incubation with sera for 12 hours at 4°C, secondary rabbit polyclonal anti-MDA antibody (catalog ab6463; Abcam) was applied for 1 hour at room temperature. Bound antigens or cytokines were detected with goat anti-rabbit IgG–HRP (catalog 4030-05; SouthernBiotech) and visualized at 450 nm using a TMB substrate (Sigma-Aldrich).

GeneChip analysis. Gene expression analysis was performed using the mouse WG-6 BeadChip and iScan system (Illumina). Total RNA FACS sorted from MZMs, gated as F4/80^{neg}CD11b^{lo}SIGN-R1$^+$I-Ab$^-$, was converted to cDNA by reverse transcription, followed by second-strand synthesis to generate double-stranded cDNA. After purification, the cDNA was converted to biotin-labeled cRNA, hybridized to a mouse WG-6 BeadChip, and stained with strepavidin-Cy3 for visualization. The mouse WG-6 BeadChips contain sequences representing approximately 45,200 curated and putative genes and expressed sequence tags (ESTs). Quality standards for hybridization, labeling, staining, background signal, and basal level of housekeeping gene expression for each chip were verified. After scanning the probe array, the resulting image was analyzed using GenomeStudio software, version 2011.1 (Illumina). Gene lists were further analyzed using GeneSpring software, version 12.1 (Agilent Technologies). Data

were analyzed using Ingenuity Pathways Analysis (IPA) (Ingenuity Systems, www.ingenuity.com). Upstream Regulator Analysis from IPA was used to identify the upstream regulators that were responsible for the gene expression changes observed in the data. The activation Z-score (an algorithm designed to reduce the chance that random data will generate significant predictions) identifies upstream regulators that can explain observed gene expression changes in the data and predicts the activation state of the upstream regulators. An absolute Z-score greater than or equal to 2 was considered significant. Predictions in which both the Z-score is significant (absolute value ≥2) and the P value is significant ($<10^{E-3}$) are the most reliable predictions. Microarray data were deposited in the NCBI's Gene Expression Omnibus (GEO) database (GEO GSE66687). Samples were derived from splenic MZMs (F4/80^{neg}CD11b^{lo}SIGN-R1$^+$I-A^{b-}) of BXD2 mice administered PBS (GSM1627971 and GSM1627972), BXD2-*Ifnar*$^{-/-}$ mice administered PBS (GSM1627973), and BXD2 mice administered sLTβR-Fc (GSM1627974). Each chip is the result of 2 spleens.

Statistics. All results are shown as the mean ± SEM. A 2-tailed, unpaired Student's *t* test was used when 2 groups were compared for statistical differences. The distribution differences of mLT$^+$ B cells in the anatomical MZ area versus those in the anatomical follicular area between different strains of mice were tested using a χ^2 test. P values of less than 0.05 were considered significant.

Study approval. All human studies were designated by the IRB of the University of Alabama at Birmingham as "Not Human Subject Research" (NHSR), since all tissues were deidentified cadaveric autopsy specimens. All animal studies were approved in by the IACUC of the University of Alabama at Birmingham.

1. Elkon KB, Silverman GJ. Naturally occurring autoantibodies to apoptotic cells. *Adv Exp Med Biol*. 2012;750:14–26.
2. Li H, et al. Cutting edge: defective follicular exclusion of apoptotic antigens due to marginal zone macrophage defects in autoimmune BXD2 mice. *J Immunol*. 2013;190(9):4465–4469.
3. Rowland SL, et al. Early, transient depletion of plasmacytoid dendritic cells ameliorates autoimmunity in a lupus model. *J Exp Med*. 2014;211(10):1977–1991.
4. Baechler EC, et al. Interferon-inducible gene expression signature in peripheral blood cells of patients with severe lupus. *Proc Natl Acad Sci U S A*. 2003;100(5):2610–2615.
5. Bennett L, et al. Interferon and granulopoiesis signatures in systemic lupus erythematosus blood. *J Exp Med*. 2003;197(6):711–723.
6. Jego G, Palucka AK, Blanck JP, Chalouni C, Pascual V, Banchereau J. Plasmacytoid dendritic cells induce plasma cell differentiation through type I interferon and interleukin 6. *Immunity*. 2003;19(2):225–234.
7. Kiefer K, Oropallo MA, Cancro MP, Marshak-Rothstein A. Role of type I interferons in the activation of autoreactive B cells. *Immunol Cell Biol*. 2012;90(5):498–504.
8. Obermoser G, Pascual V. The interferon-alpha signature of systemic lupus erythematosus. *Lupus*. 2010;19(9):1012–1019.
9. Casciola-Rosen LA, Anhalt G, Rosen A. Autoantigens targeted in systemic lupus erythematosus are clustered in two populations of surface structures on apoptotic keratinocytes. *J Exp Med*. 1994;179(4):1317–1330.
10. Fransen JH, et al. Mouse dendritic cells matured by ingestion of apoptotic blebs induce T cells to produce interleukin-17. *Arthritis Rheum*. 2009;60(8):2304–2313.
11. Peng Y, Martin DA, Kenkel J, Zhang K, Ogden CA, Elkon KB. Innate and adaptive immune response to apoptotic cells. *J Autoimmun*. 2007;29(4):303–309.
12. McGaha TL, Chen Y, Ravishankar B, van Rooijen N, Karlsson MC. Marginal zone macrophages suppress innate and adaptive immunity to apoptotic cells in the spleen. *Blood*. 2011;117(20):5403–5412.
13. Ravishankar B, et al. Tolerance to apoptotic cells is regulated by indoleamine 2,3-dioxygenase. *Proc Natl Acad Sci U S A*. 2012;109(10):3909–3914.
14. Ravishankar B, et al. Marginal zone CD169$^+$ macrophages coordinate apoptotic cell-driven cellular recruitment and tolerance. *Proc Natl Acad Sci U S A*. 2014;111(11):4215–4220.
15. Miyake Y, Asano K, Kaise H, Uemura M, Nakayama M, Tanaka M. Critical role of macrophages in the marginal zone in the suppression of immune responses to apoptotic cell-associated antigens. *J Clin Invest*. 2007;117(8):2268–2278.
16. Hsu HC, et al. Overexpression of activation-induced cytidine deaminase in B cells is associated with production of highly pathogenic autoantibodies. *J Immunol*. 2007;178(8):5357–5365.
17. Hsu HC, et al. Interleukin 17-producing T helper cells and interleukin 17 orchestrate autoreactive germinal center development in autoimmune BXD2 mice. *Nat Immunol*. 2008;9(2):18157131.
18. Hsu HC, et al. Inhibition of the catalytic function of activation-induced cytidine deaminase promotes apoptosis of germinal center B cells in BXD2 mice. *Arthritis Rheum*. 2011;63(7):2038–2048.
19. Mountz JD, Wang JH, Xie S, Hsu HC. Cytokine regulation of B-cell migratory behavior favors formation of germinal centers in autoimmune disease. *Discov Med*. 2011;11(56):76–85.
20. Wang JH, et al. Marginal zone precursor B cells as cellular agents for type I IFN-promoted antigen transport in autoimmunity. *J Immunol*. 2010;184(1):442–451.
21. Wang JH, et al. Type I interferon-dependent CD86(high) marginal zone precursor B cells are potent T cell costimulators in mice. *Arthritis Rheum*. 2011;63(4):1054–1064.
22. Shiow LR, et al. CD69 acts downstream of interferon-alpha/beta to inhibit S1P1 and lymphocyte egress from lymphoid organs. *Nature*. 2006;440(7083):540–544.
23. Allen LA, Aderem A. Molecular definition of distinct cytoskeletal structures involved in complement- and Fc receptor-mediated phagocytosis in macrophages. *J Exp Med*. 1996;184(2):627–637.
24. May RC, Machesky LM. Phagocytosis and the actin cytoskeleton. *J Cell Sci*. 2001;114(pt 6):1061–1077.
25. Fan H, Patel VA, Longacre A, Levine JS. Abnormal regulation of the cytoskeletal regulator Rho

typifies macrophages of the major murine models of spontaneous autoimmunity. *J Leukoc Biol*. 2006;79(1):155–165.

26. Cen B, Selvaraj A, Prywes R. Myocardin/MKL family of SRF coactivators: key regulators of immediate early and muscle specific gene expression. *J Cell Biochem*. 2004;93(1):74–82.

27. Smith EC, et al. MKL1 and MKL2 play redundant and crucial roles in megakaryocyte maturation and platelet formation. *Blood*. 2012;120(11):2317–2329.

28. Caron E, Hall A. Identification of two distinct mechanisms of phagocytosis controlled by different Rho GTPases. *Science*. 1998;282(5394):1717–1721.

29. Miralles F, Posern G, Zaromytidou AI, Treisman R. Actin dynamics control SRF activity by regulation of its coactivator MAL. *Cell*. 2003;113(3):329–342.

30. Mouilleron S, Guettler S, Langer CA, Treisman R, McDonald NQ. Molecular basis for G-actin binding to RPEL motifs from the serum response factor coactivator MAL. *EMBO J*. 2008;27(23):3198–3208.

31. Vartiainen MK, Guettler S, Larijani B, Treisman R. Nuclear actin regulates dynamic subcellular localization and activity of the SRF cofactor MAL. *Science*. 2007;316(5832):1749–1752.

32. Ding Y, et al. IL-17RA is essential for optimal localization of follicular Th cells in the germinal center light zone to promote autoantibody-producing B cells. *J Immunol*. 2013;191(4):1614–1624.

33. Ding Y, et al. Interleukin-21 promotes germinal center reaction by skewing the follicular regulatory T cell to follicular helper T cell balance in autoimmune BXD2 mice. *Arthritis Rheumatol*. 2014;66(9):2601–2612.

34. Hsu HC, et al. Production of a novel class of polyreactive pathogenic autoantibodies in BXD2 mice causes glomerulonephritis and arthritis. *Arthritis Rheum*. 2006;54(1):343–355.

35. Mountz JD, et al. Genetic segregation of spontaneous erosive arthritis and generalized autoimmune disease in the BXD2 recombinant inbred strain of mice. *Scand J Immunol*. 2005;61(2):128–138.

36. Wang JH, et al. Extension of the germinal center stage of B cell development promotes autoantibodies in BXD2 mice. *Arthritis Rheum*. 2013;65(10):2703–2712.

37. Xie S, et al. IL-17 activates the canonical NF-kappaB signaling pathway in autoimmune B cells of BXD2 mice to upregulate the expression of regulators of G-protein signaling 16. *J Immunol*. 2010;184(5):2289–2296.

38. Zhou Z, Niu H, Zheng YY, Morel L. Autoreactive marginal zone B cells enter the follicles and interact with CD4+ T cells in lupus-prone mice. *BMC Immunol*. 2011;12:7.

39. Lande R, et al. Neutrophils activate plasmacytoid dendritic cells by releasing self-DNA-peptide complexes in systemic lupus erythematosus. *Sci Transl Med*. 2011;3(73):73ra19.

40. Aichele P, Zinke J, Grode L, Schwendener RA, Kaufmann SH, Seiler P. Macrophages of the splenic marginal zone are essential for trapping of blood-borne particulate antigen but dispensable for induction of specific T cell responses. *J Immunol*. 2003;171(3):1148–1155.

41. Kang YS, et al. SIGN-R1, a novel C-type lectin expressed by marginal zone macrophages in spleen, mediates uptake of the polysaccharide dextran. *Int Immunol*. 2003;15(2):177–186.

42. Sang A, et al. Dysregulated cytokine production by dendritic cells modulates B cell responses in the NZM2410 mouse model of lupus. *PLoS One*. 2014;9(8):e102151.

43. Baccala R, Hoebe K, Kono DH, Beutler B, Theofilopoulos AN. TLR-dependent and TLR-independent pathways of type I interferon induction in systemic autoimmunity. *Nat Med*. 2007;13(5):543–551.

44. Moriyama Y, et al. Delta-like 1 is essential for the maintenance of marginal zone B cells in normal mice but not in autoimmune mice. *Int Immunol*. 2008;20(6):763–773.

45. Gommerman JL, Browning JL, Ware CF. The Lymphotoxin Network: orchestrating a type I interferon response to optimize adaptive immunity. *Cytokine Growth Factor Rev*. 2014;25(2):139–145.

46. Kraal G, Mebius R. New insights into the cell biology of the marginal zone of the spleen. *Int Rev Cytol*. 2006;250:175–215.

47. Lu TT, Cyster JG. Integrin-mediated long-term B cell retention in the splenic marginal zone. *Science*. 2002;297(5580):409–412.

48. Myers RC, King RG, Carter RH, Justement LB. Lymphotoxin alpha1beta2 expression on B cells is required for follicular dendritic cell activation during the germinal center response. *Eur J Immunol*. 2013;43(2):348–359.

49. Nolte MA, et al. B cells are crucial for both development and maintenance of the splenic marginal zone. *J Immunol*. 2004;172(6):3620–3627.

50. Onder L, et al. Endothelial cell-specific lymphotoxin-β receptor signaling is critical for lymph node and high endothelial venule formation.

J Exp Med. 2013;210(3):465–473.

51. Tumanov A, et al. Distinct role of surface lymphotoxin expressed by B cells in the organization of secondary lymphoid tissues. *Immunity*. 2002;17(3):239–250.

52. Pawlowski R, Rajakyla EK, Vartiainen MK, Treisman R. An actin-regulated importin α/β-dependent extended bipartite NLS directs nuclear import of MRTF-A. *EMBO J*. 2010;29(20):3448–3458.

53. Olson EN, Nordheim A. Linking actin dynamics and gene transcription to drive cellular motile functions. *Nat Rev Mol Cell Biol*. 2010;11(5):353–365.

54. Sullivan AL, et al. Serum response factor utilizes distinct promoter- and enhancer-based mechanisms to regulate cytoskeletal gene expression in macrophages. *Mol Cell Biol*. 2011;31(4):861–875.

55. Fleige A, et al. Serum response factor contributes selectively to lymphocyte development. *J Biol Chem*. 2007;282(33):24320–24328.

56. Weller S, et al. Human blood IgM "memory" B cells are circulating splenic marginal zone B cells harboring a prediversified immunoglobulin repertoire. *Blood*. 2004;104(12):3647–3654.

57. Wang DZ, et al. Potentiation of serum response factor activity by a family of myocardin-related transcription factors. *Proc Natl Acad Sci U S A*. 2002;99(23):14855–14860.

58. Johnson LA, Rodansky ES, Haak AJ, Larsen SD, Neubig RR, Higgins PD. Novel Rho/MRTF/SRF inhibitors block matrix-stiffness and TGF-β-induced fibrogenesis in human colonic myofibroblasts. *Inflamm Bowel Dis*. 2014;20(1):154–165.

59. Zhou Y, et al. Inhibition of mechanosensitive signaling in myofibroblasts ameliorates experimental pulmonary fibrosis. *J Clin Invest*. 2013;123(3):1096–1108.

60. Charras G, Sahai E. Physical influences of the extracellular environment on cell migration. *Nat Rev Mol Cell Biol*. 2014;15(12):813–824.

61. Nakaya M, Tanaka M, Okabe Y, Hanayama R, Nagata S. Opposite effects of rho family GTPases on engulfment of apoptotic cells by macrophages. *J Biol Chem*. 2006;281(13):8836–8842.

62. Chen XW, Shen Y, Sun CY, Wu FX, Chen Y, Yang CD. Anti-class a scavenger receptor autoantibodies from systemic lupus erythematosus patients impair phagocytic clearance of apoptotic cells by macrophages in vitro. *Arthritis Res Ther*. 2011;13(1):R9.

63. Wu Q, Wang Y, Wang J, Hedgeman EO, Browning JL, Fu YX. The requirement of membrane lymphotoxin for the presence of dendritic cells in lymphoid tissues. *J Exp Med*. 1999;190(5):629–638.